



On the Swerve Response of Projectiles to Control Input

by Douglas Ollerenshaw and Mark Costello

ARL-CR-0604

April 2008

prepared by

Oregon State University
Corvallis, Oregon

and

Georgia Institute of Technology
Atlanta, Georgia

under contract

W911QX-06-C-0113

NOTICES

Disclaimers

The findings in this report are not to be construed as an official Department of the Army position unless so designated by other authorized documents.

Citation of manufacturer's or trade names does not constitute an official endorsement or approval of the use thereof.

DESTRUCTION NOTICE—Destroy this report when it is no longer needed. Do not return it to the originator.

Army Research Laboratory

Aberdeen Proving Ground, MD 21005-5069

ARL-CR-0604

April 2008

On the Swerve Response of Projectiles to Control Input

Douglas Ollerenshaw

Department of Mechanical Engineering, Oregon State University

Mark Costello

School of Aerospace Engineering, Georgia Institute of Technology

prepared by

**Oregon State University
Corvallis, Oregon**

and

**Georgia Institute of Technology
Atlanta, Georgia**

under contract

W911QX-06-C-0113

REPORT DOCUMENTATION PAGE			Form Approved OMB No. 0704-0188	
Public reporting burden for this collection of information is estimated to average 1 hour per response, including the time for reviewing instructions, searching existing data sources, gathering and maintaining the data needed, and completing and reviewing the collection information. Send comments regarding this burden estimate or any other aspect of this collection of information, including suggestions for reducing the burden, to Department of Defense, Washington Headquarters Services, Directorate for Information Operations and Reports (0704-0188), 1215 Jefferson Davis Highway, Suite 1204, Arlington, VA 22202-4302. Respondents should be aware that notwithstanding any other provision of law, no person shall be subject to any penalty for failing to comply with a collection of information if it does not display a currently valid OMB control number.				
PLEASE DO NOT RETURN YOUR FORM TO THE ABOVE ADDRESS.				
1. REPORT DATE (DD-MM-YYYY) April 2008		2. REPORT TYPE Final		3. DATES COVERED (From - To) October 2006 to September 2007
4. TITLE AND SUBTITLE On the Swerve Response of Projectiles to Control Input			5a. CONTRACT NUMBER W911QX-06-C-0113	
			5b. GRANT NUMBER	
			5c. PROGRAM ELEMENT NUMBER	
6. AUTHOR(S) Douglas Ollerenshaw (OSU); Mark Costello (GIT)			5d. PROJECT NUMBER AH80	
			5e. TASK NUMBER	
			5f. WORK UNIT NUMBER	
7. PERFORMING ORGANIZATION NAME(S) AND ADDRESS(ES) Oregon State University Georgia Institute of Technology Corvallis, Oregon Atlanta, Georgia			8. PERFORMING ORGANIZATION REPORT NUMBER ARL-CR-0604	
9. SPONSORING/MONITORING AGENCY NAME(S) AND ADDRESS(ES) U.S. Army Research Laboratory Weapons and Materials Research Directorate Aberdeen Proving Ground, MD 21005-5069			10. SPONSOR/MONITOR'S ACRONYM(S)	
			11. SPONSOR/MONITOR'S REPORT NUMBER(S)	
12. DISTRIBUTION/AVAILABILITY STATEMENT Approved for public release; distribution is unlimited.				
13. SUPPLEMENTARY NOTES The contracting officer's representative (COR) is Peter Plostins, U.S. Army Research Laboratory, ATTN: AMSRD-ARL-WM-BC, Aberdeen Proving Ground, MD 21005-5069, telephone number (410) 306-0800.				
14. ABSTRACT The swerve response of fin- and spin-stabilized projectiles to control mechanism input is sometimes not intuitive and often surprises smart weapon designers. This report seeks to explain the basic parameters that govern swerve of projectiles excited by control input. By modeling the overall effect of any control mechanism as a non-rolling reference frame force or moment applied to the projectile, we obtain general expressions for swerve in terms of basic vehicle parameters. These compact expressions are used to show that maximum swerve response for a fin-stabilized projectile is achieved when the force is applied near the nose of the projectile, while maximum swerve response for a spin-stabilized projectile is achieved when the force is applied near the base of the projectile.				
15. SUBJECT TERMS guidance navigation and control; swerve response				
16. SECURITY CLASSIFICATION OF:			17. LIMITATION OF ABSTRACT SAR	18. NUMBER OF PAGES 30
a. REPORT UNCLASSIFIED	b. ABSTRACT UNCLASSIFIED	c. THIS PAGE UNCLASSIFIED		
			19b. TELEPHONE NUMBER (Include area code) 410-306-0800	

Contents

List of Figures	iv
List of Tables	iv
1. Introduction	1
2. Simplified Analytical Swerve Solution	1
3. Correlation to Full Six-Degree-of-Freedom Model	9
4. Effects of Individual Parameters	15
5. Conclusions	19
6. References	20
Distribution List	22

List of Figures

Figure 1. Vertical plane swerve response of the M829A2 fin-stabilized projectile to 1-lbf control input applied in the +y, +z, -y, and -z directions, with 6-DOF correlation data.....	11
Figure 2. Magnitude of the swerve response of the M829A2 fin-stabilized projectile to a 1-lbf control input as a function of the distance from the projectile c.g. to the point of application of the force, with 6-DOF correlation data.	12
Figure 3. Phase shift of the swerve response of the M829A2 fin-stabilized projectile to a 1-lbf control input as a function of the distance from the projectile c.g. to the point of application of the force, with 6-DOF correlation data.	12
Figure 4. Vertical plane swerve response of the M549 spin-stabilized projectile to 1-lbf control input applied in the +y, +z, -y, and -z directions, with 6-DOF correlation data.....	13
Figure 5. Magnitude of the swerve response of the M549 spin-stabilized projectile to a 1-lbf control input as a function of the distance from the projectile c.g. to the point of application of the force, with 6-DOF correlation data.	14
Figure 6. Phase shift of the swerve response of the M549 spin-stabilized projectile to a 1-lbf control input as a function of the distance from the projectile c.g. to the point of application of the force, with 6-DOF correlation data.	14
Figure 7. Summary of projectile response to a control input in the positive y-direction in both a fin-stabilized and a spin-stabilized projectile.....	17
Figure 8. Magnitude of the swerve response of the M549 spin-stabilized projectile to a 1-lbf control input as a function of the distance from the projectile c.g. to the point of application of the control force, Magnus force coefficient varied from its value to zero.....	18
Figure 9. Phase shift of the swerve response of the M549 spin-stabilized projectile to a 1-lbf control input as a function of the distance from the projectile c.g. to the point of application of the control force, Magnus force coefficient varied from its value to zero.....	18

List of Tables

Table 1. Summary of projectile initial conditions, physical parameters, and aerodynamic coefficients.	10
--	----

1. Introduction

The continuing development of micro-electromechanical systems (MEMS) is pointing to the possibility of mounting complete sensor systems on medium and small caliber projectiles as part of an actively controlled smart munition. Two important technical challenges in achieving this goal are the development of small, rugged sensor suites and control mechanisms. There is currently a flurry of activity to create innovative physical control mechanisms. Concepts include pulse jets, squibs, synthetic jets (1, 2, 3), drag brakes (4, 5), deployable pins (6, 7), movable nose (8), movable canards (9), dual-spin projectiles (10, 11), ram air deflection (12), and internal translating mass (13), to name a few.

Although the physical control mechanisms mentioned are very diverse, there is a common theme among all these physical control mechanisms. All concepts exert a force and/or moment on the projectile. Moreover, since trajectories are shaped relative to ground coordinates, the forces and moments are effectively applied in a non-rolling reference frame. Although the uncontrolled dynamics of projectiles (both fin stabilized and spin stabilized) have been extensively studied in the ballistics community (14), issues with regard to control response have received considerably less attention because of the lack of practical application of control technology to spinning projectiles. With the use of projectile linear theory, this report analytically investigates several aspects of the response of a spinning projectile to a control force and/or moment in the non-rolling reference frame. Simple expressions result for the swerve response magnitude and phase angle in terms of basic physical mass properties, aerodynamic characteristics, and the state of the air vehicle. These expressions provide a means toward deeper understanding of the underlying factors driving control response of projectiles, helping smart weapon designers to create more capable weapon systems.

2. Simplified Analytical Swerve Solution

The six-degree-of-freedom (6-DOF) rigid body dynamic model used to simulate the trajectory of a projectile in atmospheric flight has been well developed. The model consists of the three inertial components of the position vector from an inertial frame to the projectile mass center and the three standard Euler orientation angles. The resulting equations of motion are shown as equations 1 through 4 (15).

$$\begin{Bmatrix} \dot{x} \\ \dot{y} \\ \dot{z} \end{Bmatrix} = \begin{bmatrix} c_\theta c_\psi & s_\phi s_\theta c_\psi - c_\phi s_\psi & c_\phi s_\theta c_\psi + s_\phi s_\psi \\ c_\theta s_\psi & s_\phi s_\theta s_\psi + c_\phi c_\psi & c_\phi s_\theta s_\psi - s_\phi c_\psi \\ -s_\theta & s_\phi c_\theta & c_\phi c_\theta \end{bmatrix} \begin{Bmatrix} u \\ v \\ w \end{Bmatrix} \quad (1)$$

$$\begin{Bmatrix} \dot{\phi} \\ \dot{\theta} \\ \dot{\psi} \end{Bmatrix} = \begin{bmatrix} 1 & s_{\phi}t_{\theta} & c_{\phi}t_{\theta} \\ 0 & c_{\phi} & -s_{\phi} \\ 0 & s_{\phi}/c_{\theta} & c_{\phi}/c_{\theta} \end{bmatrix} \begin{Bmatrix} p \\ q \\ r \end{Bmatrix} \quad (2)$$

$$\begin{Bmatrix} \dot{u} \\ \dot{v} \\ \dot{w} \end{Bmatrix} = \begin{Bmatrix} X/m \\ Y/m \\ Z/m \end{Bmatrix} - \begin{bmatrix} 0 & -r & q \\ r & 0 & -p \\ -q & p & 0 \end{bmatrix} \begin{Bmatrix} u \\ v \\ w \end{Bmatrix} \quad (3)$$

$$\begin{Bmatrix} \dot{p} \\ \dot{q} \\ \dot{r} \end{Bmatrix} = [I]^{-1} \begin{Bmatrix} L \\ M \\ N \end{Bmatrix} - \begin{bmatrix} 0 & -r & q \\ r & 0 & -p \\ -q & p & 0 \end{bmatrix} [I] \begin{Bmatrix} p \\ q \\ r \end{Bmatrix} \quad (4)$$

In equations 1 and 2, the standard shorthand notation for trigonometric functions is used: $\sin(\alpha) \equiv s_{\alpha}$, $\cos(\alpha) \equiv c_{\alpha}$, and $\tan(\alpha) \equiv t_{\alpha}$. The forces and moments appearing in equations 3 and 4 contain contributions from weight, body aerodynamics, and control forces and are discussed in detail in the literature (16).

Since no analytical solution can be found for the differential equations shown, they must be solved with numerical integration techniques. Over time, however, a series of simplifications of the dynamic equations has been identified, which results in an analytically solvable set of quasi-linear differential equations and reasonably accurate trajectories. These equations are referred to collectively as projectile linear theory (17). The dynamic equations that constitute projectile linear theory are given as equations 5 through 13.

$$\begin{Bmatrix} \tilde{v}' \\ \tilde{w}' \\ \tilde{q}' \\ \tilde{r}' \end{Bmatrix} = \begin{bmatrix} -A & 0 & 0 & -D \\ 0 & -A & D & 0 \\ \frac{B}{D} & \frac{C}{D} & H & -F \\ -\frac{C}{D} & \frac{B}{D} & F & H \end{bmatrix} \begin{Bmatrix} \tilde{v} \\ \tilde{w} \\ \tilde{q} \\ \tilde{r} \end{Bmatrix} + \begin{Bmatrix} V_F \\ W_F \\ Q_F \\ R_F \end{Bmatrix} \quad (5)$$

$$V' = \frac{\pi\rho D^3 C_{x0}}{8m} V - \frac{gD\theta}{V} \quad (6)$$

$$p' = \frac{\pi\rho D^4 C_{LDD}}{8I_x} V + \frac{\pi\rho D^5 C_{LP}}{16I_x} p \quad (7)$$

$$\phi' = Dp \quad (8)$$

$$\theta' = \frac{D}{V} \tilde{q} \quad (9)$$

$$\psi' = \frac{D}{V} \tilde{r} \quad (10)$$

$$x' = D \quad (11)$$

$$y' = \frac{D}{V} \tilde{v} + \psi D \quad (12)$$

$$z' = \frac{D}{V} \tilde{w} - \theta D \quad (13)$$

The projectile linear theory dynamic equations use dimensionless arc length, s , as the independent variable. Arc length is related to time as shown in equation 14:

$$s = \frac{1}{D} \int_0^t V dt \quad (14)$$

Additionally, the linear theory equations employ a reference frame that is aligned with the projectile axis of symmetry but does not roll. Variables in this reference frame, referred to as the no-roll frame or the fixed plane frame, are denoted with a \sim superscript. The no-roll frame is related to the body fixed frame used in the traditional 6-DOF equations by a single axis rotation about the projectile axis of symmetry. For example, the no-roll frame velocity components are related to the body frame velocity components as shown in equation 15:

$$\begin{Bmatrix} \tilde{u} \\ \tilde{v} \\ \tilde{w} \end{Bmatrix} = \begin{bmatrix} 1 & 0 & 0 \\ 0 & c_\phi & -s_\phi \\ 0 & s_\phi & c_\phi \end{bmatrix} \begin{Bmatrix} u \\ v \\ w \end{Bmatrix} \quad (15)$$

For the purpose of examining basic swerve response attributable to control input, gravity and atmospheric winds are neglected. The constant terms in the set of four coupled equations shown as equation 5, referred to as the epicyclic equations, can then be described as

$$A = \frac{\pi\rho D^3 C_{NA}}{8m} \quad (16)$$

$$B = \frac{\pi\rho D^5 C_{YPA} p \Delta_{SLM}}{16I_p V} \quad (17)$$

$$C = \frac{\pi\rho D^4 C_{NA} \Delta_{SLP}}{8I_p} \quad (18)$$

$$F = \frac{I_R D p}{I_p V} \quad (19)$$

$$H = \frac{\pi\rho D^5 C_{MQ}}{16I_p} \quad (20)$$

$$V_F = \frac{DY_C}{mV} \quad (21)$$

$$W_F = \frac{DZ_C}{mV} \quad (22)$$

$$Q_F = -\frac{D\Delta_{SLC}Z_C}{I_pV} \quad (21)$$

$$R_F = \frac{D\Delta_{SLC}Y_C}{I_pV} \quad (22)$$

Both the velocity (V) and the roll rate (p) are considered to be constant wherever they appear in equations 9 through 13 and equations 16 through 22. The terms D and m refer to the projectile reference diameter and the total projectile mass, respectively. The projectile inertia terms, I_p and I_R , are respectively the roll and pitch inertias. The term ρ is the atmospheric air density. The term C_{NA} is the normal force coefficient. The normal force acts in a direction perpendicular to the projectile axis of symmetry and results from non-axial wind forces caused by yawing and pitching of the projectile. The normal force acts not at the projectile center of gravity (c.g.) but at a point called the normal force center of pressure (COP). The Δ_{SLP} term represents the distance between the c.g. and the center of pressure as follows:

$$\Delta_{SLP} = SL_{COP} - SL_{CG} \quad (23)$$

in which both the c.g. and the center of pressure are measured from the projectile base along the projectile stationline. C_{YPA} is the Magnus force coefficient. The Magnus force is caused by unequal pressures on opposite sides of a spinning body resulting from the viscous interaction between the spinning surface and the surrounding atmosphere. The Magnus force itself is generally considered to be small enough to be neglected. However, the resulting moment must be considered. Δ_{SLM} represents the distance between the c.g. and the point of application of the Magnus force (MAG):

$$\Delta_{SLM} = SL_{MAG} - SL_{CG} \quad (24)$$

in which both the c.g. and the MAG application point are measured from the projectile base along the projectile stationline. The MAG is proportional to both spin rate and transverse angular velocity. Therefore, in projectiles with very low spin rates, the Magnus moment approaches zero. The term C_{MQ} represents the pitch-damping moment coefficient. The pitch-damping moment is proportional to the transverse angular velocity of the projectile. C_{MQ} will always be negative for a stable projectile. Thus, it has the stabilizing effect of decreasing the total transverse angular velocity of the projectile.

Finally, the terms Y_C and Z_C represent applied control forces applied along the y and z axes of the projectile no-roll frame. Both forces are assumed to act at the same point (CF) on the projectile with a moment arm, Δ_{SLC} , defined as

$$\Delta_{SLC} = SL_{CF} - SL_{CG} \quad (25)$$

in which both the center of mass and the point of application of the control forces are measured from the rear of the projectile along the projectile axis of symmetry.

Determining the solution of the coupled epicyclic equations is necessary before solving both the attitude (θ, ψ) and the swerve (y, z) equations. To obtain the solution, the epicyclic equations are first transformed into the Laplace domain.

$$\begin{Bmatrix} \tilde{v}(s) \\ \tilde{w}(s) \\ \tilde{q}(s) \\ \tilde{r}(s) \end{Bmatrix} = \begin{bmatrix} s+A & 0 & 0 & D \\ 0 & s+A & -D & 0 \\ -\frac{B}{D} & -\frac{C}{D} & s-H & F \\ \frac{C}{D} & -\frac{B}{D} & F & s-H \end{bmatrix}^{-1} \begin{Bmatrix} \tilde{v}(0) + \frac{V_F}{s} \\ \tilde{w}(0) + \frac{W_F}{s} \\ \tilde{q}(0) + \frac{Q_F}{s} \\ \tilde{r}(0) + \frac{R_F}{s} \end{Bmatrix} \quad (26)$$

It is important to note that the variable s as expressed in equation 24 is the Laplace operator, not arc length as described in equation 14. Equation 26 can be expanded so that each of the four expressions, represented by the dummy variable ζ , is in the following form

$$\zeta(s) = \frac{\eta_{\zeta 4}s^4 + \eta_{\zeta 3}s^3 + \eta_{\zeta 2}s^2 + \eta_{\zeta 1}s + \eta_{\zeta 0}}{s^5 + \delta_{\zeta 4}s^4 + \delta_{\zeta 3}s^3 + \delta_{\zeta 2}s^2 + \delta_{\zeta 1}s + \delta_{\zeta 0}} \quad (27)$$

in which $\eta_{\zeta 4}, \eta_{\zeta 3}, \eta_{\zeta 2}, \eta_{\zeta 1}, \eta_{\zeta 0}, \delta_{\zeta 4}, \delta_{\zeta 3}, \delta_{\zeta 2}, \delta_{\zeta 1}, \delta_{\zeta 0}$ are all known constants expressed in terms of the epicyclic initial conditions and the constants $A, B, C, F, H, V_F, W_F, Q_F, R_F$. The non-zero eigenvalues of the system are broken into two pairs of complex conjugates known as the fast and slow modes of the system. They are described as

$$\lambda_F = \frac{1}{2}(-A + H \pm iF) + \frac{1}{2}\sqrt{A^2 \pm 4iB + 4C \pm 2iAF - F^2 + 2AH \pm 2iFH + H^2} \quad (28)$$

$$\lambda_S = \frac{1}{2}(-A + H \pm iF) - \frac{1}{2}\sqrt{A^2 \pm 4iB + 4C \pm 2iAF - F^2 + 2AH \pm 2iFH + H^2} \quad (29)$$

Thus, each term can also be written in partial fractions form as

$$\zeta(s) = \frac{C_{\zeta 0}}{s} + \frac{F_{\zeta 1}s + F_{\zeta 0}}{s^2 + 2\zeta_F \omega_F s + \omega_F^2} + \frac{S_{\zeta 1}s + S_{\zeta 0}}{s^2 + 2\zeta_S \omega_S s + \omega_S^2} \quad (30)$$

in which the fast and slow mode natural frequencies and damping rates are described as

$$\omega_F = \sqrt{\lambda_{F1}\lambda_{F2}} \quad (31)$$

$$\zeta_F = -\frac{(\lambda_{F1} + \lambda_{F2})}{2\sqrt{\lambda_{F1}\lambda_{F2}}} \quad (32)$$

$$\omega_S = \sqrt{\lambda_{S1}\lambda_{S2}} \quad (33)$$

$$\zeta_S = -\frac{(\lambda_{S1} + \lambda_{S2})}{2\sqrt{\lambda_{S1}\lambda_{S2}}} \quad (34)$$

Equations 27 and 30 can be equated to one another, with the resulting expression used to solve for the unknown coefficients in the numerator of equation 30. The generalized Laplace domain solution for each of the four epicyclic differential equations can also be expressed as shown in equation 35.

$$\begin{aligned} \zeta(s) = & \frac{C_{\zeta 0}}{s} + F_{\zeta 1} \left(\frac{s - \lambda_{FR}}{(s - \lambda_{FR})^2 + \lambda_{FI}^2} \right) + F_{\zeta 1} \left(\frac{\frac{F_{\zeta 0}}{F_{\zeta 1}} + \lambda_{FR}}{(s - \lambda_{FR})^2 + \lambda_{FI}^2} \right) \\ & + S_{\zeta 1} \left(\frac{s - \lambda_{SR}}{(s - \lambda_{SR})^2 + \lambda_{SI}^2} \right) + S_{\zeta 1} \left(\frac{\frac{S_{\zeta 0}}{S_{\zeta 1}} + \lambda_{SR}}{(s - \lambda_{SR})^2 + \lambda_{SI}^2} \right) \end{aligned} \quad (35)$$

in which λ_{FR} and λ_{FI} are the real and imaginary parts of the fast mode eigenvalues, and λ_{SR} and λ_{SI} are the real and imaginary parts of the slow mode eigenvalues. Note that equation 35 is arranged to match standard forms found in inverse Laplace transform tables, thus allowing easy transformation of the epicyclic solutions back to the arc length domain.

With the epicyclic solutions thus obtained, the attitude solutions can be expressed in the Laplace domain as

$$\psi(s) = \frac{D}{V_S} \tilde{r}(s) + \frac{1}{s} \psi(0) \quad (36)$$

$$\theta(s) = \frac{D}{V_S} \tilde{q}(s) + \frac{1}{s} \theta(0) \quad (37)$$

Similarly, the swerve solutions can be expressed in the Laplace domain as

$$y(s) = \frac{D}{V_S} \tilde{v}(s) + \frac{D}{s} \psi(s) + \frac{1}{s} y(0) \quad (38)$$

$$z(s) = \frac{D}{V_S} \tilde{w}(s) - \frac{D}{s} \theta(s) + \frac{1}{s} z(0) \quad (39)$$

The attitude expressions shown in equations 36 and 37, along with the expressions for $\tilde{v}(s)$, $\tilde{w}(s)$, $\tilde{q}(s)$, and $\tilde{r}(s)$, as expressed in equation 35, can be substituted into the swerve expressions in equations 38 and 39. Taking the inverse Laplace transform of the resulting expressions yields arc length domain swerve solutions of the form

$$y(s) = C_{y0} + C_{y1}s + C_{y2}s^2 + e^{\lambda_{FR}s} (C_{yfc} \cos(\lambda_{FI}s) + C_{yfs} \sin(\lambda_{FI}s)) + e^{\lambda_{SR}s} (C_{ysc} \cos(\lambda_{SI}s) + C_{yss} \sin(\lambda_{SI}s)) \quad (40)$$

$$z(s) = C_{z0} + C_{z1}s + C_{z2}s^2 + e^{\lambda_{FR}s} (C_{zfc} \cos(\lambda_{FI}s) + C_{zfs} \sin(\lambda_{FI}s)) + e^{\lambda_{SR}s} (C_{zsc} \cos(\lambda_{SI}s) + C_{zss} \sin(\lambda_{SI}s)) \quad (41)$$

Additionally, the down-range position of the projectile, x , expressed as a function of arc length is simply

$$x(s) = x_0 + Ds \quad (42)$$

One must be careful to note that the s term appearing in equations 40 through 41 represents arc length, as defined in equation 14.

To obtain a sense of the generalized swerve response of a projectile because of applied control forces, we examine the case in which the projectile is fired down range with no initial pitch or yaw angle and with no initial perturbations of the transverse lateral and angular velocities. Assuming that the firing position is at the origin of the inertial reference frame, this allows us to set the initial conditions of all terms to zero, except for velocity and roll rate. The velocity and roll rate initial conditions are denoted V_0 and p_0 . Additionally, as stated earlier, the effects of gravity and atmospheric winds are neglected here. These assumptions provide a case in which a projectile with no control forces applied displays no swerving motion. Subsequently, the swerve response created by the application of control forces will be clear.

When we examine the swerve expressions in equations 40 and 41, a few simplifications can be made. First of all, note that in a stable projectile, the real parts of the fast and slow mode eigenvalues, λ_{FR} and λ_{SR} , are always negative. Therefore, the oscillatory terms in the swerve response decays as the projectile flies down range and can be neglected for long-term swerve response. The pitch-damping moment is primarily associated with the oscillatory epicyclic terms and can also be neglected, allowing C_{MQ} in equation 20 to be set to zero. Additionally, as the arc length value becomes large, the terms containing the square of the arc length begin to dominate the swerve response expressions and the terms C_{y0} , C_{y1} , C_{z0} , and C_{z1} can be neglected. Finally, equation 42 can be solved for arc length, s , and substituted into equations 40 and 41.

The resulting simplified swerve expressions can then be expressed as a function of range solely in terms of projectile parameters, initial velocity, and spin rate, and control force input applied in

the no-roll frame. They can be further simplified if we express the swerve response in terms of its magnitude relative to the magnitude of the control input, and the phase shift relative to the angle of the applied control vector. A compact and informative expression for the response magnitude, R , results:

$$R = \frac{F_C x^2}{2V_0^2} \sqrt{\frac{D^2 p_0^2 C_{YPA}^2 \Delta_{SLM}^2 + 4V_0^2 C_{NA}^2 (\Delta_{SLC} - \Delta_{SLP})^2}{p_0^2 (2I_R C_{NA} + mDC_{YPA} \Delta_{SLM})^2 + 4m^2 V_0^2 C_{NA}^2 \Delta_{SLP}^2}} \quad (43)$$

in which F_C is the magnitude of the control force, defined as

$$F_C = \sqrt{F_y^2 + F_z^2} \quad (44)$$

The expression for the phase shift of the swerve response, Φ_R , is

$$\Phi_R = \tan^{-1} \left(\frac{2V_0 p_0 C_{NA} (2I_R C_{NA} (\Delta_{SLC} - \Delta_{SLP}) + mDC_{YPA} \Delta_{SLM} \Delta_{SLC})}{Dp_0^2 C_{YPA} \Delta_{SLM} (2I_R C_{NA} + mDC_{YPA} \Delta_{SLM}) - 4mV_0^2 C_{NA}^2 \Delta_{SLP} (\Delta_{SLC} - \Delta_{SLP})} \right) \quad (45)$$

The phase angle of the swerve response, Φ_T , in the y - z plane can be found if we add the phase angle of the control input to the phase shift of the swerve response, Φ_R , as follows:

$$\Phi_T = \tan^{-1} \left(\frac{F_z}{F_y} \right) + \Phi_R \quad (46)$$

Since the inverse tangent function will only result in values between $-\pi/2$ and $\pi/2$, careful consideration must be paid to the signs of the numerator and denominator of the arguments in equations 46 and 47 to ensure that the result is in the proper quadrant of the y - z plane. It is advisable to use the *atan2* function instead to avoid confusion.

Equations 43 and 45 can be further simplified if the control mechanism being investigated imparts only a pure moment upon the projectile body. The expression for the swerve response magnitude, R , becomes

$$R = \frac{M_C x^2 C_{NA}}{V_0} \sqrt{\frac{1}{p_0^2 (2I_R C_{NA} + mDC_{YPA} \Delta_{SLM})^2 + 4m^2 V_0^2 C_{NA}^2 \Delta_{SLP}^2}} \quad (47)$$

in which M_C is the magnitude of the applied control moment, defined as

$$M_C = \sqrt{M_y^2 + M_z^2} \quad (48)$$

The phase shift of the swerve response, Φ_R , becomes

$$\Phi_R = \tan^{-1} \left(\frac{2mV_0 C_{NA} \Delta_{SLP}}{p_0 (2I_R C_{NA} + mDC_{YPA} \Delta_{SLM})} \right) \quad (49)$$

As before, the phase angle of the swerve response, Φ_T , in the y - z plane can be found if we add the phase angle of the control input to the phase shift of the swerve response, Φ_R .

$$\Phi_T = \tan^{-1}\left(\frac{M_z}{M_y}\right) + \Phi_R \quad (50)$$

These equations provide relatively compact expressions for the swerve magnitude (equations 43 and 47) and swerve phase angle (equations 45 and 49) because of a control force applied to a point on the projectile (equations 43 and 45) and a pure moment applied to the projectile (equations 47 and 49). These expressions highlight the key parameters that drive control response of projectiles excited by control force and moment input. However, when one is applying these formulas, it is important to recall that stability of the projectile is inherent in the assumptions used to achieve these expressions. When parameters are varied in these expressions to investigate the effects on swerve response, care must be taken to ensure that the stability assumption is not violated. It also needs to be emphasized that these equations calculate the magnitude and phase shift of the swerve response under the assumption that the velocity and spin rate remain constant at their initial values, and in turn, all Mach number dependent quantities remain constant as well. Of course, this assumption becomes increasingly inaccurate as the projectile proceeds down range and must be periodically updated for long-range trajectories.

3. Correlation to Full Six-Degree-of-Freedom Model

To demonstrate the accuracy of the simplified swerve equations obtained previously, two exemplar projectiles were chosen for which complete body aerodynamic properties are already known. The two projectiles chosen were the M829A2 fin-stabilized projectile and M549 spin-stabilized projectile. For both projectiles, the results obtained with equations 43 and 45 were compared to results from a fixed step, fourth order Runge-Kutta numerical integration of the full 6-DOF equations of motion given as equations 1 through 4. For both projectiles, the swerve response was evaluated at a range of 5,280 feet in the absence of gravity and atmospheric winds and with no initial yaw or pitch angle. In both cases, four input force scenarios were examined: $F_y = 1$ lbf & $F_z = 0$ lbf, $F_y = 0$ lbf & $F_z = 1$ lbf, $F_y = -1$ lbf & $F_z = 0$ lbf, and $F_y = 0$ lbf & $F_z = -1$ lbf. The control force moment arm, Δ_{SLC} , in equations 43 and 45 was varied from 1 foot behind the projectile center of mass to 1 foot in front of the projectile center of mass. The 6-DOF swerve response was calculated for each input force scenario with control force moment arms of $\Delta_{SLC} = -1.0$ ft, $\Delta_{SLC} = -0.5$ ft, $\Delta_{SLC} = 0.0$ ft, $\Delta_{SLC} = 0.5$ ft, and $\Delta_{SLC} = 1.0$ ft. The 6-DOF expressions calculate all forces and moments in the projectile body frame, as opposed to the projectile no-roll frame used to achieve the swerve expressions presented here. Therefore, the control forces and moments must be transformed from the no-roll frame to the body frame for use in the 6-DOF expressions.

Table 1 summarizes the initial conditions and the resultant aerodynamic coefficients, along with the relevant physical parameters, for both projectiles as used in equations 43 and 45.

Table 1. Summary of projectile initial conditions, physical parameters, and aerodynamic coefficients.

	M829A2	M549
V_o (ft/s)	5479.0	2710.0
p_o (rad/s)	8.7000	1674.1
ρ (slug/ft ³)	2.3785×10^{-3}	2.3785×10^{-3}
I_R (slug*ft ²)	2.3870×10^{-4}	0.10857
I_P (slug*ft ²)	0.17718	1.3964
m (slug)	0.34461	2.9465
D (ft)	0.08790	0.50853
C_{NA}	13.350	2.6314
C_{YPA}	0.0000	-0.9600
C_{MQ}	-5215.8	-27.700
Δ_{SLM} (ft)	-1.3833	-0.52920
Δ_{SLP} (ft)	-0.50079	-0.71373

Figure 1 shows the swerve response of the M829A2 fin-stabilized projectile in the vertical target plane at a down-range location of $x = 5280$ ft, with five 6-DOF data points included to demonstrate correlation. Note that the positive z -direction points downward in the negative altitude direction. Figures 2 and 3 show the magnitude and phase shift of the response, along with 6-DOF correlation data for the M829A2. Note that the magnitude of the response depends only upon the magnitude of the control input, not its direction. The phase shift of the response, however, does not vary with the magnitude of the input and also depends on the direction of the input force. As positive y is rightward and positive z is downward in the vertical target plane plots, a positive phase shift is in the clockwise direction.

Figure 4 shows the swerve response of the M529 spin-stabilized projectile in the vertical target plane at a down-range location of $x = 5280$ ft, with five 6-DOF data points included to demonstrate correlation. Figures 5 and 6 show the magnitude and phase shift of the response, along with 6-DOF correlation data for the M549.

For both the fin-stabilized and spin-stabilized projectiles studied here, the response as predicted by the simplified swerve equations is shown to correlate very well with that predicted by the full 6-DOF simulation at this relatively short range. Though only a very small fraction of the total terms comprising the full linear theory swerve expressions are preserved in the simplified version presented, it is obvious that those terms providing the dominant effect on the swerve response have been retained.

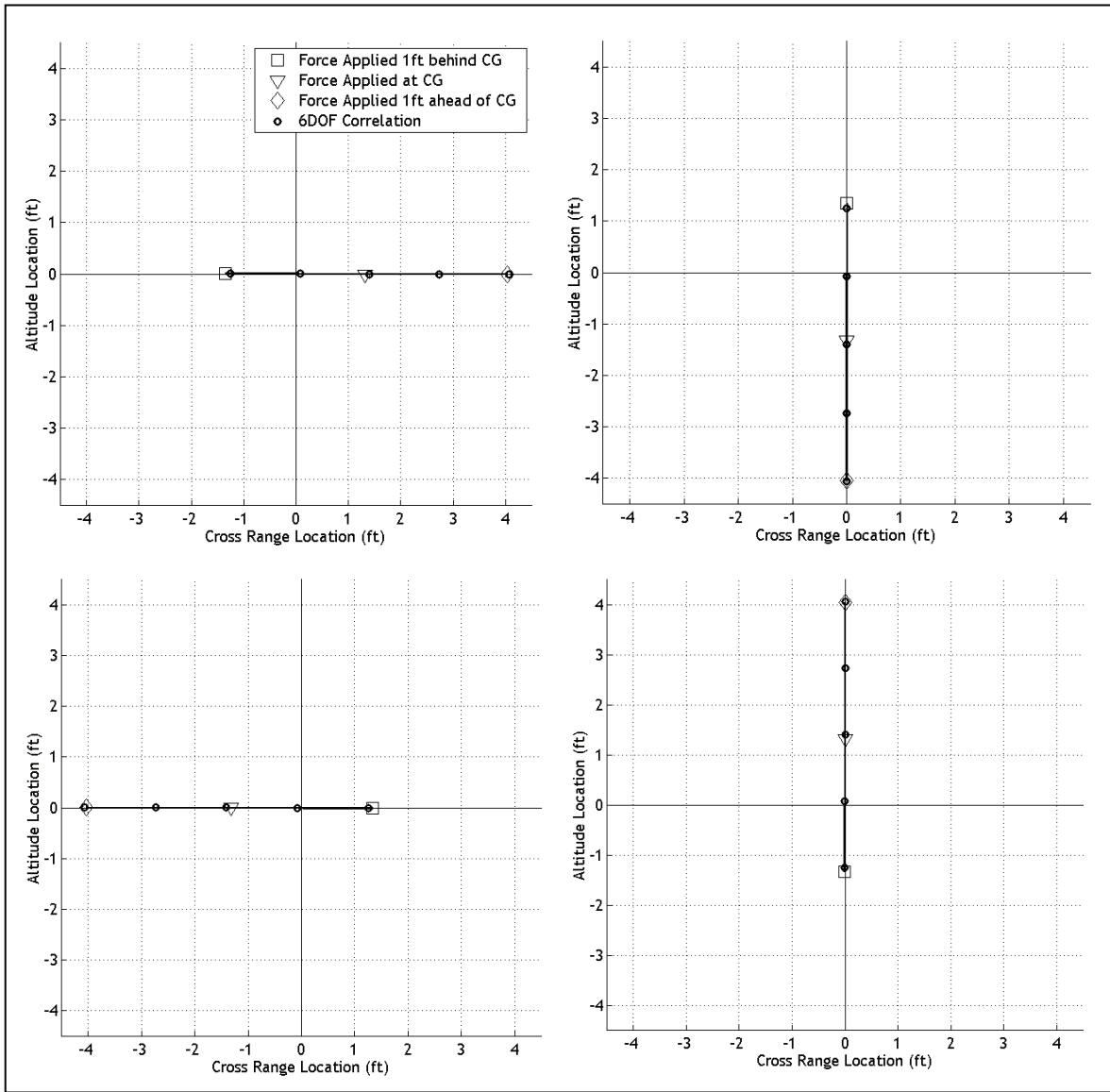


Figure 1. Vertical plane swerve response of the M829A2 fin-stabilized projectile to 1-lbf control input applied in the +y, +z, -y, and -z directions, with 6-DOF correlation data.

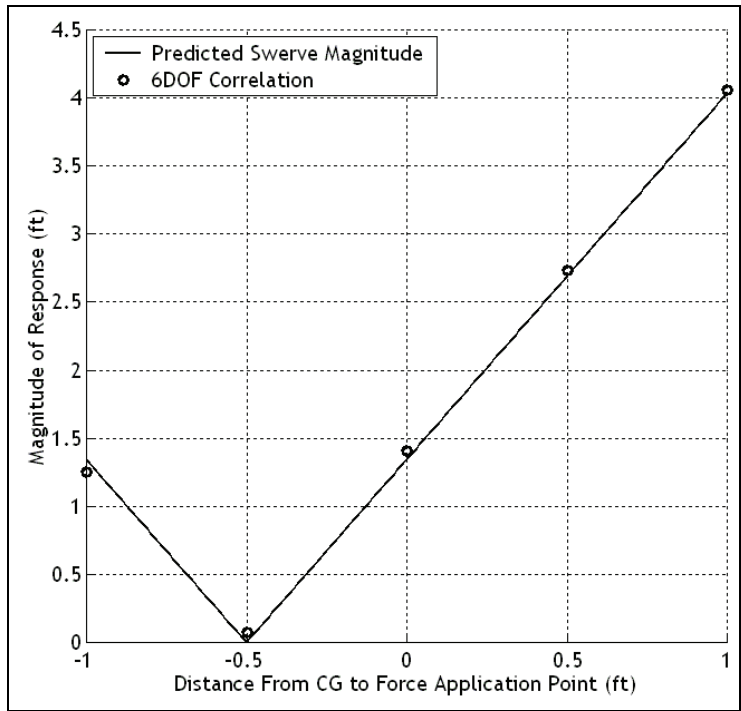


Figure 2. Magnitude of the swerve response of the M829A2 fin-stabilized projectile to a 1-lbf control input as a function of the distance from the projectile c.g. to the point of application of the force, with 6-DOF correlation data.

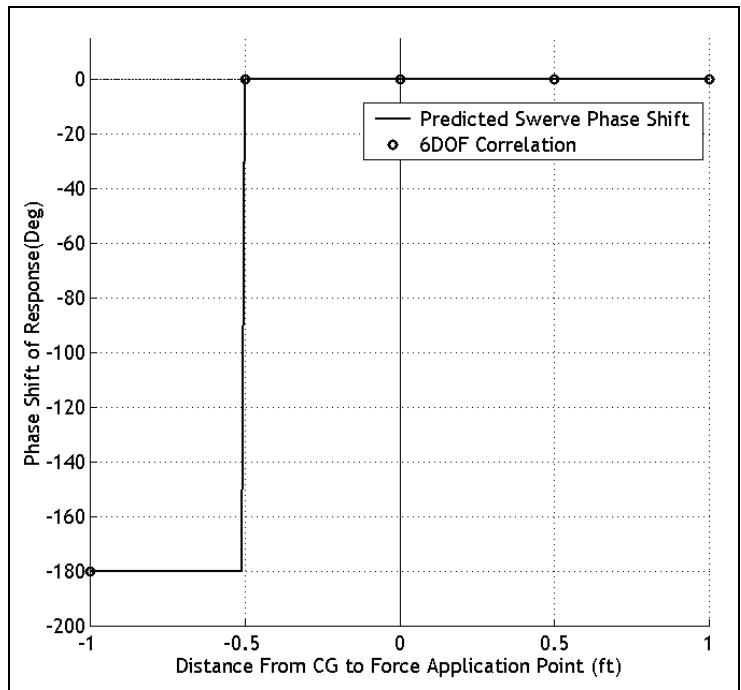


Figure 3. Phase shift of the swerve response of the M829A2 fin-stabilized projectile to a 1-lbf control input as a function of the distance from the projectile c.g. to the point of application of the force, with 6-DOF correlation data.

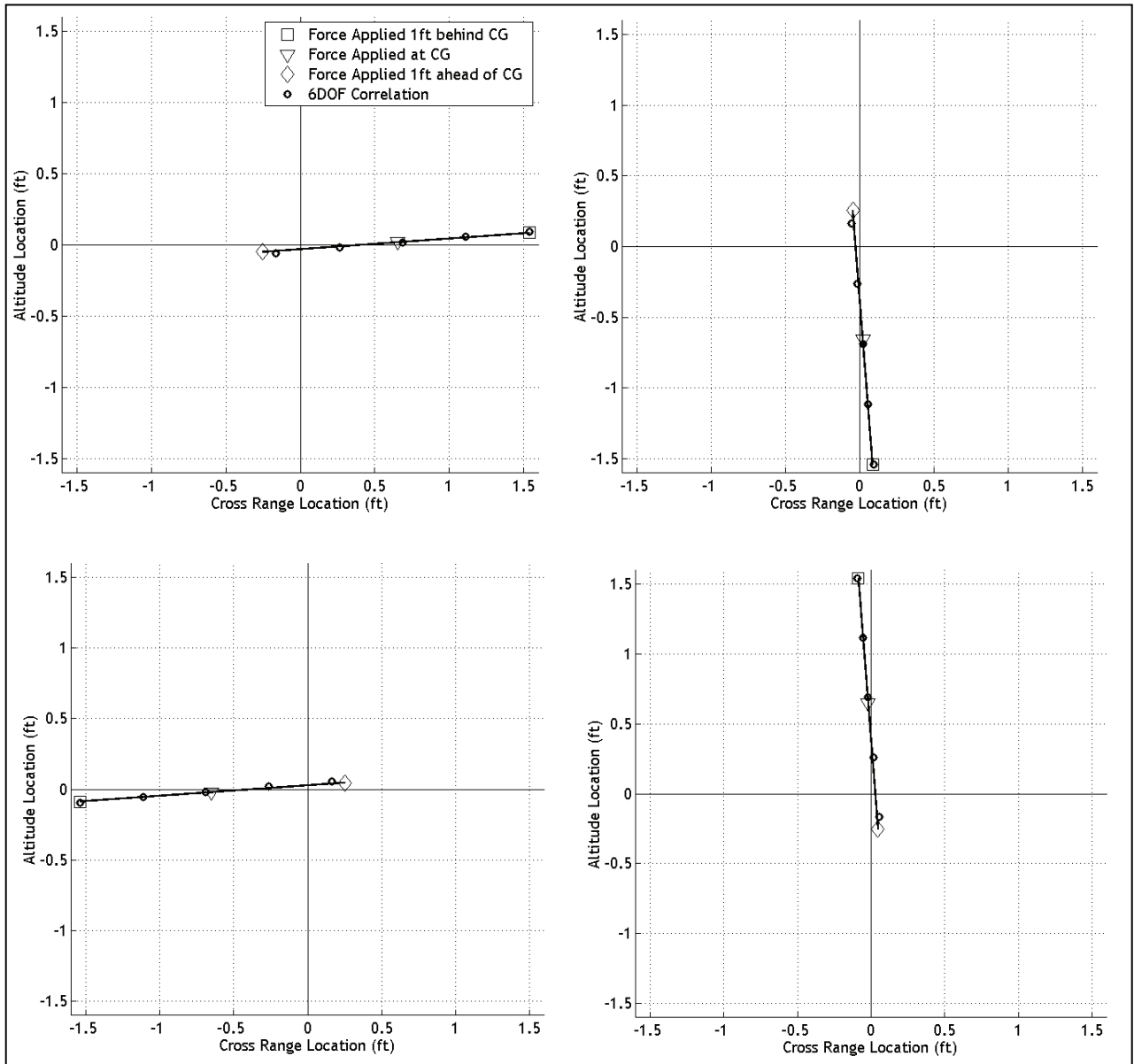


Figure 4. Vertical plane swerve response of the M549 spin-stabilized projectile to 1-lbf control input applied in the +y, +z, -y, and -z directions, with 6-DOF correlation data.

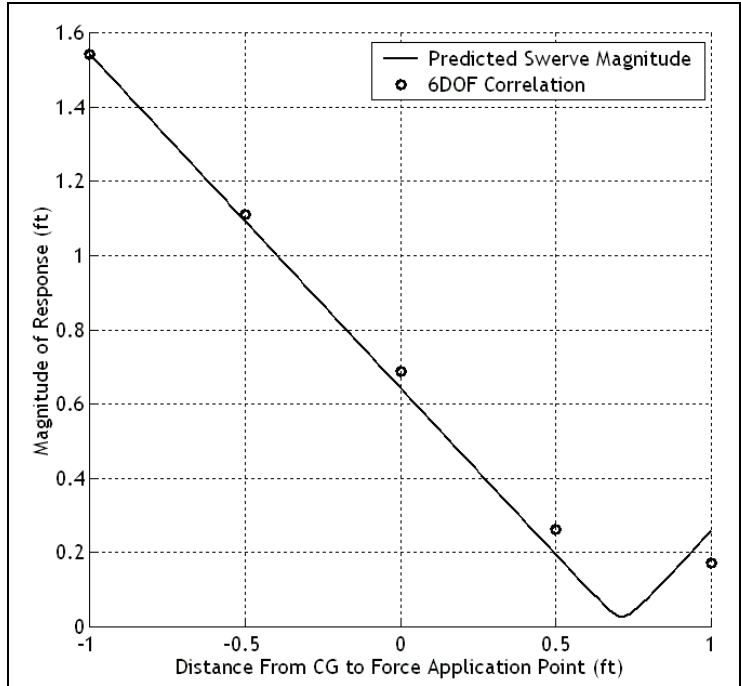


Figure 5. Magnitude of the swerve response of the M549 spin-stabilized projectile to a 1-lbf control input as a function of the distance from the projectile c.g. to the point of application of the force, with 6-DOF correlation data.

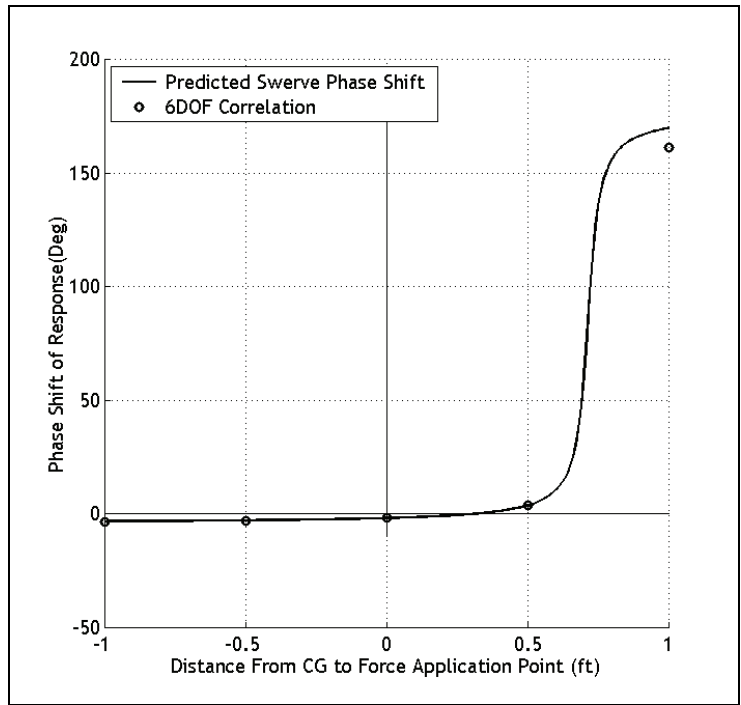


Figure 6. Phase shift of the swerve response of the M549 spin-stabilized projectile to a 1-lbf control input as a function of the distance from the projectile c.g. to the point of application of the force, with 6-DOF correlation data.

4. Effects of Individual Parameters

Figures 1 through 6 clearly show that the point of application of the control force has a very large effect on both the direction and the magnitude of the swerve response. Further, they demonstrate that the effects are drastically different for fin- and spin-stabilized projectiles. The simplified swerve expressions provide insight into the physical reasons for this behavior. In the swerve response magnitude and phase expressions given as equations 43 and 45, the term expressing the distance from the center of pressure location to the point of application of the control force, $(\Delta_{SLC} - \Delta_{SLP})$, appears repeatedly. The practical result is that if control force is applied at the center of pressure, $(\Delta_{SLC} - \Delta_{SLP})$ becomes zero and the response magnitude is at a minimum. In the case of a fin-stabilized projectile, which has very low spin rates and negligibly small Magnus effects as a result, the magnitude of the response goes to zero when the control force is applied at the center of pressure.

The direction of the response is also driven by the center of pressure. A typical fin-stabilized projectile will have a center of pressure behind the projectile center of mass, resulting in a negative Δ_{SLP} . A control force applied in front of the center of pressure leads to $(\Delta_{SLC} - \Delta_{SLP})$ becoming positive. This will result in a positive numerator and a much larger positive denominator, indicating a very small positive phase shift. Conversely, when the control force is applied behind the center pressure, $(\Delta_{SLC} - \Delta_{SLP})$ becomes negative and so do the numerator and denominator of equation 45. This indicates a phase shift of nearly -180 degrees.

A spin-stabilized projectile displays the opposite behavior, resulting from the center of pressure being typically located ahead of the center of mass. With a positive Δ_{SLP} , a control force applied in front of the center of pressure will result in a positive numerator and a negative denominator in equation 45, indicating a phase shift approaching 180 degrees out of phase with the direction of the applied force. When the control force is applied behind the center of mass, the response will be approximately in phase with the direction of the applied force. The Magnus moment causes a comparably smaller response which is 90 degrees out of phase with the direction of the applied control force.

Equations 47 and 49, the expressions for swerve response magnitude and phase shift in terms of pure applied moments, can be analyzed similarly. For a fin-stabilized projectile, a positive moment will lead to a response -90 degrees out of phase with the direction of the applied moment. For instance, a positive moment in projectile no-roll z -direction will lead to a response in the positive y -direction. A spin-stabilized projectile will respond in the opposite direction to the same applied moment. Again, this effect can be tied directly to the sign of Δ_{SLP} in equation 49.

The physical explanation for this behavior is relatively simple. Application of a control force away from the c.g., or application of a pure control moment, creates a non-zero angle of attack in

the projectile. The normal force results directly from the angle of attack and, in a stable projectile, will create a moment equal and opposite to the moment caused by the control input. The direction of the response will be driven primarily by the sum of these two forces. If the sum of the control force and the normal force are positive, the response will be in the positive direction. When the control force is applied at the center of pressure, the normal force will be equal and opposite to the control force and the response will be driven solely by the Magnus effect, which only persists in spin-stabilized projectiles. If the sum of the two forces is negative, the response will be in the negative direction. When a pure moment is applied to a projectile without an applied control force, the normal force alone determines the direction of the response. In the case of a fin-stabilized projectile, with a center of pressure behind the center of mass, a positive normal force is necessary to counteract a positive applied control moment, leading to a response in the positive direction. The opposite occurs in a spin-stabilized projectile. Figure 7 graphically summarizes the effects of a control force in the positive y-direction applied at varying points on the projectile body.

To demonstrate the relatively small contribution of the Magnus moment in a spin-stabilized projectile, figures 8 and 9 show the predicted swerve magnitude and phase shift, respectively, of the M549 projectile when the Magnus force coefficient is equal to -0.96, -0.48, and 0.

The magnitude of the response is largely unaffected if the Magnus moment reduced or removed, except when the control force is applied near the projectile center of pressure. When that is the case, the normal force is near zero and the Magnus moment becomes the dominant factor in the response magnitude. When the Magnus moment is neglected entirely, the magnitude of response of the M549 becomes zero when the control force is applied at the center of pressure, as is the case in a fin-stabilized projectile.

The effect of the Magnus moment becomes more apparent when we examine the phase response of the M549 with varied Magnus force coefficients. The Magnus moment acts 90 degrees out of phase with the angle of attack of the projectile. As the Magnus force coefficient is reduced, the portion of the response that is orthogonal to the control input diminishes. With no Magnus moment present, the response is almost completely in phase with a force applied behind the center of pressure and is nearly 180 degrees out of phase for a force applied in front of the center of pressure.

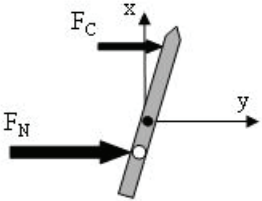
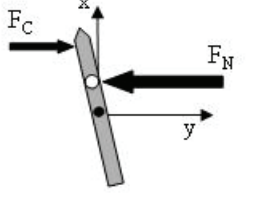
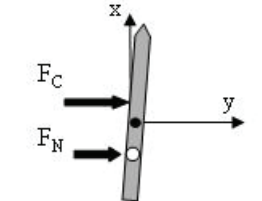
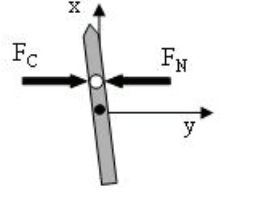
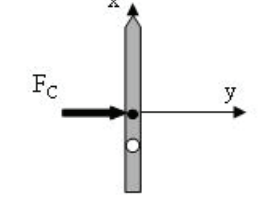
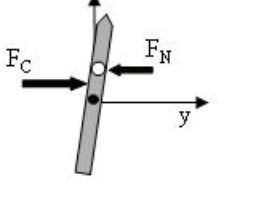
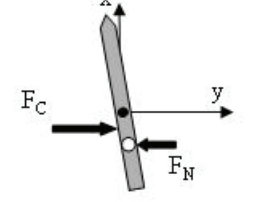
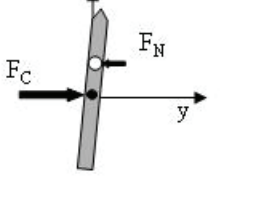
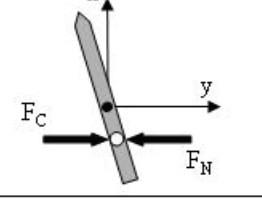
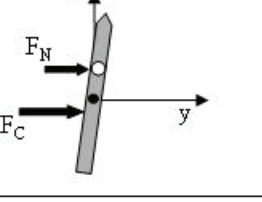
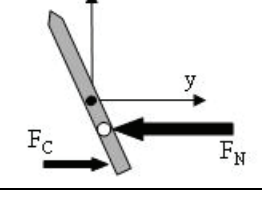
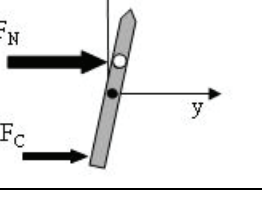
<p align="center">Fin Stabilized Projectile</p> <p align="center">Center of Pressure (shown in white) is behind of Center of Mass (shown in black)</p>	<p align="center">Spin Stabilized Projectile</p> <p align="center">Center of Pressure (shown in white) is ahead of Center of Mass (shown in black)</p>
 <p> $\Delta_{szc} > 0$ $\Delta_{szc} > \Delta_{szp}$ $\tilde{\nu} < 0 \therefore F_N > 0$ $\psi > 0$ $(F_C + F_N) > 0$ $\therefore \text{Swerve Response} > 0$ </p>	 <p> $\Delta_{szc} > 0$ $\Delta_{szc} > \Delta_{szp}$ $\tilde{\nu} > 0 \therefore F_N < 0$ $\psi < 0$ $(F_C + F_N) < 0$ $\text{Swerve Response} < 0$ </p>
 <p> $\Delta_{szc} > 0$ $\Delta_{szc} < \Delta_{szp}$ $\tilde{\nu} < 0 \therefore F_N > 0$ $\psi > 0$ $(F_C + F_N) > 0$ $\therefore \text{Swerve Response} > 0$ </p>	 <p> $\Delta_{szc} > 0$ $\Delta_{szc} = \Delta_{szp}$ $\tilde{\nu} > 0 \therefore F_N < 0$ $\psi < 0$ $(F_C + F_N) = 0$ $\therefore \text{Swerve Response} = 0$ </p>
 <p> $\Delta_{szc} = 0$ $\tilde{\nu} = 0 \therefore F_N = 0$ $\psi = 0$ $(F_C + F_N) > 0$ $\therefore \text{Swerve Response} > 0$ </p>	 <p> $\Delta_{szc} > 0$ $\Delta_{szc} < \Delta_{szp}$ $\tilde{\nu} > 0 \therefore F_N < 0$ $\psi > 0$ $(F_C + F_N) > 0$ $\therefore \text{Swerve Response} > 0$ </p>
 <p> $\Delta_{szc} < 0$ $\Delta_{szc} < \Delta_{szp}$ $\tilde{\nu} > 0 \therefore F_N < 0$ $\psi < 0$ $(F_C + F_N) > 0$ $\therefore \text{Swerve Response} > 0$ </p>	 <p> $\Delta_{szc} = 0$ $\tilde{\nu} > 0 \therefore F_N < 0$ $\psi > 0$ $(F_C + F_N) > 0$ $\therefore \text{Swerve Response} > 0$ </p>
 <p> $\Delta_{szc} < 0$ $\Delta_{szc} = \Delta_{szp}$ $\tilde{\nu} > 0 \therefore F_N < 0$ $\psi < 0$ $(F_C + F_N) = 0$ $\therefore \text{Swerve Response} = 0$ </p>	 <p> $\Delta_{szc} < 0$ $\Delta_{szc} < \Delta_{szp}$ $\tilde{\nu} < 0 \therefore F_N > 0$ $\psi > 0$ $(F_C + F_N) > 0$ $\therefore \text{Swerve Response} > 0$ </p>
 <p> $\Delta_{szc} < 0$ $\Delta_{szc} > \Delta_{szp}$ $\tilde{\nu} > 0 \therefore F_N < 0$ $\psi < 0$ $(F_C + F_N) < 0$ $\therefore \text{Swerve Response} < 0$ </p>	 <p> $\Delta_{szc} < 0$ $\Delta_{szc} > \Delta_{szp}$ $\tilde{\nu} < 0 \therefore F_N > 0$ $\psi > 0$ $(F_C + F_N) > 0$ $\therefore \text{Swerve Response} > 0$ </p>

Figure 7. Summary of projectile response to a control input in the positive y-direction in both a fin-stabilized and a spin-stabilized projectile. (Magnus moments, which act 90 degrees out of phase with the angle of attack in spin-stabilized projectiles, are not shown.)

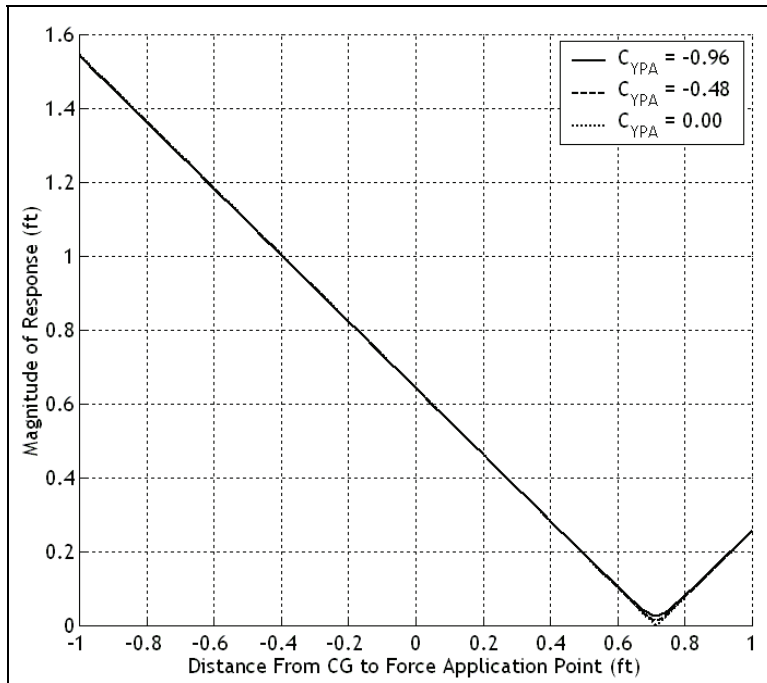


Figure 8. Magnitude of the swerve response of the M549 spin-stabilized projectile to a 1-lbf control input as a function of the distance from the projectile c.g. to the point of application of the control force, Magnus force coefficient varied from -0.96 to 0.

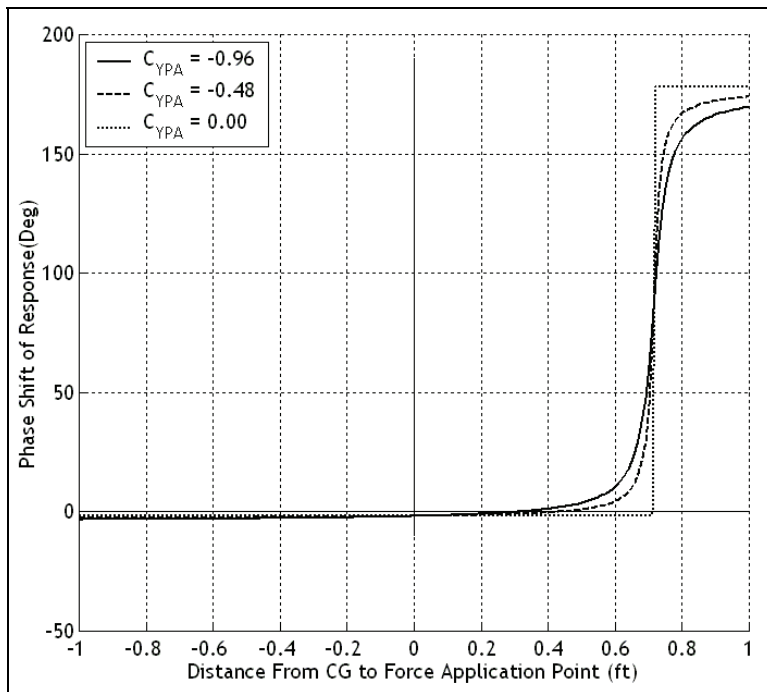


Figure 9. Phase shift of the swerve response of the M549 spin-stabilized projectile to a 1-lbf control input as a function of the distance from the projectile c.g. to the point of application of the control force, Magnus force coefficient varied from -0.96 to 0.

5. Conclusions

Relatively simple, closed form formulas for the magnitude and phase angle of a projectile excited by control forces or moments in terms of fundamental projectile flight mechanic parameters have been created. The swerve response formulas are remarkably accurate, given the litany of simplifications and the resulting compact form of the results. These formulas explain in a clear manner the control response differences between fin- and spin-stabilized projectiles, including the key role that the center of pressure plays in control force response. It is shown that fin-stabilized projectiles, respond in phase to control force input forward of the center of pressure and control moments, while spin-stabilized projectiles respond out of phase to control force input forward of the center of pressure and control moments. The simple formulas reported here are expected to be useful to smart weapon designers in bringing to light basic parameters that drive swerve response from different control mechanisms.

6. References

1. Harkins, T.; Brown, T. *Using Active Damping as a Precision-Enhancing Technology for 2.75-Inch Rockets*; ARL-TR-1772; U.S. Army Research Laboratory, Aberdeen Proving Ground, MD, 1999.
2. Jitraphai, T.; Costello, M. Dispersion Reduction of a Direct Fire Rocket Using Lateral Pulse Jets. *Journal of Spacecraft and Rockets* **2001**, 38 (6), 929-936.
3. Amitay, M.; Smith, D.; Kibens, V.; Parekh, D.; Glezer, A. Aerodynamic Flow Control Over an Unconventional Airfoil Using Synthetic Jet Actuators. *AIAA Journal* **2001**, 39 (3), 361-370.
4. Harkins, T.; Davis, B. Drag-Brake Deployment Method and Apparatus for Range Error Correction of Spinning, Gun-Launched Artillery Projectiles, United States Patent 6345785, 2002.
5. Hillstrom, T.; Osborne, P. United Defense Course Correcting Fuze for the Precision Guidance Kit Program. *49th NDIA Annual Fuze Conference*, April 5-7, 2005.
6. Massey, K.; Flick, A. Mechanical and Jet Actuators for Guiding a Small Caliber Subsonic Projectile, AIAA Paper AIAA-2007-3813, *25th AIAA Applied Aerodynamics Conference*, Miami, FL, June 25-28, 2007.
7. Massey, K.; McMichael, J.; Warnock, T.; Hay, F. Mechanical Actuators for Guidance of a Supersonic Projectile," AIAA Paper AIAA-2005-4970, *23rd AIAA Applied Aerodynamics Conference*, Toronto, Ontario, June 6-9, 2005.
8. Costello, M.; Agarwalla, R. Improved Dispersion of a Fin Stabilized Projectile using a Passive Moveable Nose. *Journal of Guidance, Control, and Dynamics* **2002**, 23 (5), 900-903, 2000. Errata: Vol 25, No 2, pp 414.
9. Costello, M. Extended Range of a Gun Launched Smart Projectile Using Controllable Canards. *Shock and Vibration* **2001**, 8 (3-4), 203-213.
10. Costello, M.; Peterson, A. Linear Theory of a Dual Spin Projectile in Atmospheric Flight. *Journal of Guidance, Control, and Dynamics* **2000**, 23 (4), 789-797.
11. Burchett, B.; Peterson, A.; Costello, M. Prediction of Swerving Motion of a Dual-Spin Projectile with Lateral Pulse Jets in Atmospheric Flight. *Mathematical and Computer Modeling* **2002**, 35 (7-8), 821-834.

12. Chandgadkar, S.; Costello, M.; Dano, B.; Liburdy, J.; Pence, D. Performance of a Smart Direct Fire Projectile Using a Ram Air Control Mechanism. *Journal of Dynamic Systems, Measurement, and Control* **2002**, *164*, 606-612.
13. Rogers, J.; Costello, M. Control Authority of a Projectile Equipped with an Internal Translating Mass. Paper Number AIAA 2007-6492, *Proceedings of the 2007 AIAA Atmospheric Flight Mechanics Conference*, Hilton Head, SC, 2007.
14. Murphy, C. H. *Free Flight Motion of Symmetric Missiles*; BRL Report No. 1216; U.S. Army Ballistic Research Laboratories, Aberdeen Proving Ground, MD, 1963.
15. Costello, M.; Anderson, D. Effect of Internal Mass Unbalance on the Terminal Accuracy and Stability of a Projectile. AIAA Paper Number 96-3447, *Proceedings of the 1996 AIAA Flight Mechanics Conference*, San Diego, CA, 1996.
16. McCoy, R. L. *Modern Exterior Ballistics: the Launch and Flight Dynamics of Symmetric Projectiles*; Schiffer Publishing Ltd., Atglen, PA, 1999.
17. Hainz, L.; Costello, M. Modified Projectile Linear Theory for Rapid Trajectory Prediction. *Journal of Guidance, Control, and Dynamics* **2005**, *28* (5), 1006-1014.

<u>NO. OF COPIES</u>	<u>ORGANIZATION</u>
1 (PDF ONLY)	DEFENSE TECHNICAL INFORMATION CTR DTIC OCA 8725 JOHN J KINGMAN RD STE 0944 FORT BELVOIR VA 22060-6218
1	US ARMY RSRCH DEV & ENGRG CMD SYSTEMS OF SYSTEMS INTEGRATION AMSRD SS T 6000 6TH ST STE 100 FORT BELVOIR VA 22060-5608
1	DIRECTOR US ARMY RESEARCH LAB IMNE ALC IMS 2800 POWDER MILL RD ADELPHI MD 20783-1197
1	DIRECTOR US ARMY RESEARCH LAB AMSRD ARL CI OK TL 2800 POWDER MILL RD ADELPHI MD 20783-1197
1	DIRECTOR US ARMY RESEARCH LAB AMSRD ARL CS OK T 2800 POWDER MILL RD ADELPHI MD 20783-1197
4	GEORGIA TECH RSCH INST ATTN J MCMICHAEL K MASSEY A LOVAS M HEIGES 7220 RICHARDSON ROAD SMYRNA GA 30080
1	USAMCOM ATTN AMSAM RD MG J BAUMANN REDSTONE ARSENAL AL 35898-5000
1	USAMCOM ATTN AMSRD AMR SG SD B NOURSE REDSTONE ARSENAL AL 35898-5000
1	AFRL/MNGN ATTN GREGG ABATE 101 W EGLIN BLVD STE 332 EGLIN AFB FL 32542
1	DR WILLIAM DAMICO 11100 JOHNS HOPKINS RD APPLIED PHYSICS LABORATORY LAUREL MD 20723-6099

<u>NO. OF COPIES</u>	<u>ORGANIZATION</u>
1	GEORGIA TECH DANIEL GUGGENHEIM SCHOOL OF AEROSPACE ENGINEERING ATTN DR MARK COSTELLO 270 FERST DRIVE ATLANTA GA 30332-0150
1	US AMRDEC ATTN AMSAM RD SS AT R KRETZSCHMAR BLDG 5400 REDSTONE ARSENAL AL 35898-5000
1	US RDECOM AMRDEC ATTN AMSRD AMR SG CT S DUNBAR BLDG 5400 REDSTONE ARSENAL AL 35898
1	US RDECOM ATTN AMSRD AMR SG SD J LOCKER BLDG 5400 REDSTONE ARSENAL AL 35898-5000
4	COMMANDER ARDEC ATTN AMSRD AAR AEM L D OKKEN R BRYAN M HORVATH P BRISLIN BLDG 65S PICATINNY ARSENAL NJ 07806-5000
2	COMMANDER ARDEC ATTN AMSRD AAR AEM M LUCIANO M PALATHINGAL BLDG 65S PICATINNY ARSENAL NJ 07806-5000
2	COMMANDER ARDEC ATTN AMSRD AAR AEP E CHRIS STOUT D CARLUCCI BLDG 94 PICATINNY ARSENAL NJ 07806-5000
1	COMMANDER ARDEC ATTN AMSRD AAR AEM J G FLEMING BLDG 65N PICATINNY ARSENAL NJ 07806-5000
1	COMMANDER ARDEC ATTN AMSRD AAR AEM D G MOSHIER BLDG 65N PICATINNY ARSENAL NJ 07806-5000

<u>NO. OF COPIES</u>	<u>ORGANIZATION</u>	<u>NO. OF COPIES</u>	<u>ORGANIZATION</u>
1	COMMANDER ARDEC ATTN AMSRD AAR AIS SA D ERICSON BLDG 12 PICATINNY ARSENAL NJ 07806-5000	1	COMMANDER US ARMY TACOM ADRDEC ATTN AMSRD AAR AEM L R SAYER BLDG 65 PICATINNY ARSENAL NJ 07806-5000
1	PROJECT MANAGER TANK MAIN ARMAMENT SYS ATTN SFAE GCSS TMA D GUZIEWICZ BLDG 354 PICATINNY ARSENAL NJ 07806-5000	1	COMMANDER US ARMY TACOM ADRDEC ATTN SFAE AMO MAS LC F CHANG BLDG 65 PICATINNY ARSENAL NJ 07806-5000
1	APM SMALL & MEDIUM CALIBER AMMO OPM MAS ATTN SFAE GCSS TMA G DEROSA BLDG 354 PICATINNY ARSENAL NJ 07806-5000	1	COMMANDER US ARMY TACOM ADRDEC ATTN AMSTA AR CCH B S PATEL BLDG 65 PICATINNY ARSENAL NJ 07806-5000
1	COMMANDER US ARMY TACOM ARDEC ATTN SFAE GCSS MAS SMC R KOWALSKI BLDG 354 PICATINNY ARSENAL NJ 07806-5000	1	COMMANDER US ARMY TACOM ATTN SFAE GCSS W AB QT COL J MORAN WARREN MI 48397-5000
3	COMMANDER US ARMY TACOM ARDEC ATTN AMSTA AR FSP P P MAGNOTTI A LICHTENBERG SCALON BLDG 61S PICATINNY ARSENAL NJ 07806-5000	3	COMMANDER US ARMY TACOM ATTN SFAE GCSS W LTC S COOPER J NEFF J FLECK WARREN MI 48397-5000
1	COMMANDER US ARMY TACOM ARDEC ATTN AMSRD AAR A MUSALLI BLDG 65S PICATINNY ARSENAL NJ 07806-5000	1	COMMANDER US ARMY TACOM ATTN SFAE CSS TV LTC R GROLLER WARREN MI 48397-5000
2	COMMANDER US ARMY TACOM ARDEC ATTN AMSRD AAR AEM L G KOLASA A MOUNA BLDG 65S PICATINNY ARSENAL NJ 07806-5000	1	DIRECTOR US ARMY ARMOR CTR ATTN ATZK TS W MEINSHAUSEN FT KNOX KY 40121
13	COMMANDER US ARMY TACOM ARDEC ATTN AMSRD AAR AEM A G LIVECCHIA J GRAU G MALEJKO E VAZQUEZ W TOLEDO L YEE R TROHANOWSKY S HAN W KOENIG S CHUNG C WILSON BLDG 95 PICATINNY ARSENAL NJ 07806-5000	2	SFSJM-CDL HQ US ARMY JOINT MUNITIONS CMD ATTN AMSIO SMT W HARRIS M RIVERS 1 ROCK ISLAND ARSENAL ROCK ISLAND IL 61299-6000
		2	DIRECTOR BENET LABORATORIES ATTN AMSTA AR CCB J VASILAKIS R HASENBEIN WATERVLIET NY 12189

NO. OF
COPIES ORGANIZATION

1 DIRECTOR
 BENET LABORATORIES
 ATTN AMSTA AR CCB RA G PFLEGL
 WATERVLIET NY 12189

2 DIRECTOR
 MARINE CORPS PROGRAMS DEPT
 NAV SURF WARCENDIC CRANE
 ATTN M O'MALLEY M STEINHOFF
 700 AMMUNITION RD
 FALLBROOK CA 92028-3187

ABERDEEN PROVING GROUND

1 DIRECTOR
 US ARMY RSCH LABORATORY
 ATTN AMSRD ARL CI OK (TECH LIB)
 BLDG 4600

32 DIRECTOR
 US ARMY RSCH LABORATORY
 ATTN AMSRD ARL WM P PLOSTINS (5 CYS)
 AMSRD ARL WM B M ZOLTOSKI
 J NEWILL
 AMSRD ARL WM BA D LYON
 T BROWN D HEPNER B DAVIS
 G KATULKA
 AMSRD ARL WM BC J SAHU
 P WEINACHT B GUIDOS (10 CYS)
 S SILTON I CELMINS G COOPER
 J DESPIRITO J GARNER M BUNDY
 B HOWELL
 AMSRD ARL WM SG W CIEPIELA